Chapter 13
Periodical Oscillations of Microseisms before the Sumatra Earthquake of December 26, 2004

G. Sobolev and A. Lyubushin

13.1 Introduction

This work continues a series of papers published in *Izvestiya, Physics of the Solid Earth*, in 2003–2006 and devoted to the detection and study of periodic oscillations in the seismic flow and synchronization effects arising before strong earthquakes [Sobolev, 2003, 2004; Sobolev et al., 2005; Sobolev and Lyubushin, 2006; Lyubushin and Sobolev, 2006]. These studies were essentially based on the concepts of the dynamics of nonequilibrium media, including self-organization of the seismic process [Nicolis and Prigogine, 1977; Bak et al., 1989; Sornette and Sammis, 1995; Ott, 2002]. It is assumed that, in a metastable lithosphere immediately before an earthquake, natural periodic oscillations arise and/or oscillations from external sources are selectively amplified, with the microseismic field showing collective behavior.

Processing of 20-Hz records obtained at the Petropavlovsk IRIS station before the Kronotskii earthquake revealed waves at periods of a few tens of minutes in the microseismic flow (Fig. 13.1). These were observable during the last 2.5 days before the main shock after the onset of foreshock activation (the arrow F in Fig. 13.1) and after the two strongest ($M > 5$) foreshocks, Fa and Fb.

To analyze the periodic structure of microseisms, we examined the time series of seismic pulses exceeding a certain level. The time series were processed with a moving time window. Within each window, a low frequency trend was removed from the records by an orthogonal polynomial of a fairly high order. After the trend removal for a given window, we calculated a threshold equal to the product of the absolute median deviation (the median of the modulus of deviations from the median) and a certain coefficient (a parameter of the method), usually varying from 1 to 4. This parameter depends on the intensity of pulses in the signal and is

G. Sobolev (✉) and A. Lyubushin
Schmidt Institute of Physics of the Earth, Russian Academy of Sciences, Moscow, Russia
e-mail: sobolev@ifz.ru; lyubushin@yandex.ru

V. de Rubeis et al. (eds.), *Synchronization and Triggering: from Fracture to Earthquake Processes*, GeoPlanet: Earth and Planetary Sciences 1,
DOI 10.1007/978-3-642-12300-9_13,

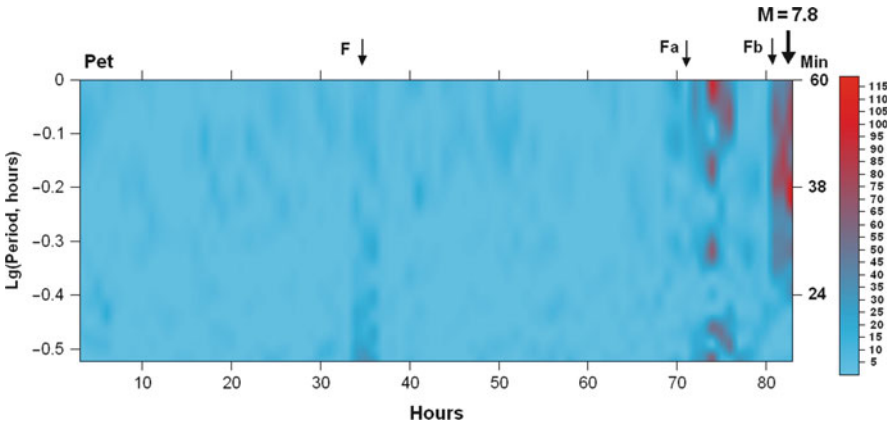

Fig. 13.1 Spectral–time diagram of the increment in the logarithmic function of likelihood $\Delta \ln L$ of microseisms at the Petropavlovsk (Pet) station. The vertical axes show the spectral period (on the right) in minutes and its logarithm (on the left). The large arrow indicates the time of the Kronotskii earthquake of December 5, 1997, with a magnitude of 7.8. The smaller arrows F, Fa, and Fb indicate the onset of foreshock activation and the two strongest foreshocks with $M > 5$

chosen experimentally. Next, we examined the sequence of the times of local maximums of the record that exceeded this threshold. Thus, the initial time series were reduced to a point process, a sequence of time moments. The latter are similar to the sequence of events in a seismic catalog. Further, we applied the method of the identification of periodic components in a sequence of events proposed in [Lyubushin et al., 1998]. We considered the model of the intensity of the event sequence (in the given case, the times of significant local maximums, i.e., pulsations of a microseismic time series), presumably containing the harmonic component

$$\lambda(t) = \mu \cdot (1 + a \cdot \cos(\omega t + \varphi)), \tag{13.1}$$

where the frequency ω, amplitude a, $0 \leq a \leq 1$, phase angle φ, $\varphi \in [0, 2\pi]$, and factor $\mu \geq 0$, (describing the Poisson part of the intensity) are model parameters. Thus, the Poisson part of the intensity is modeled by harmonic oscillations. If a richer intensity model (compared to that for a random flow of events) with a harmonic component of a given frequency ω is considered, the associated increment in the logarithmic function of likelihood is

$$\Delta \mathrm{In}L(a, \varphi|\omega) = \sum_{t_i} \ln(1 + a\cos(\omega t_i + \varphi)) + N\ln(\omega T/[\omega T + a(\sin(\omega T + \varphi) - \sin(\varphi))]) \tag{13.2}$$

Here t_i is the sequence of time moments of sufficiently large local maximums of the signal within the window, N is their number, and T is the window width.

Let

$$R(\omega) = \max_{a,\varphi} \Delta \ln L(a, \varphi|\omega), \quad 0 \leq a \leq 1, \ \varphi \in [0, 2\pi] \tag{13.3}$$

Function (13.3) can be regarded as a generalization of the spectrum for a sequence of events [Lyubushin et al., 1998]. The plot of this function illustrates how advantageous the periodic intensity model is in comparison with the purely random model. The maximum values of function (13.3) specify frequencies that are present in the flow of events. Let τ be the time of the right-hand end of the moving time window of a given width T_W. Expression (13.3) is actually a function of two arguments, $R(\omega, \tau|T_W)$, that can be visualized as 2-D maps or a 3-D relief on the plane of arguments (ω, τ). By using this frequency–time diagram, it is possible to examine the dynamics of the appearance and development of periodic components within the flow of events under study [Lyubushin, 2002; Sobolev, 2004]. It was established [Sobolev et al., 2005] that waves appeared only at the Petropavlovsk station, which was nearest to the Kronotskii earthquake epicenter (the epicentral distance $R \approx 310$ km), and were not identified in records of more remote stations (Yuzhno-Sakhalinsk, Yakutsk, and Obninsk). As the time of the Kronotskii earthquake approached, the number of predominant periods at the Petropavlovsk station decreased, so that the multimode spectrum was transformed into a unimodal spectrum, with shorter periods disappearing; 1 h before the earthquake, a period of 37 min was best expressed.

Another phenomenon recorded before the Kronotskii earthquake was the appearance of asymmetric pulses, a few minutes long [Sobolev et al., 2005]. They were observed as pulses of predominantly negative polarity that arose five days before the earthquake and three days before the onset of foreshock activation. This type of anomaly was typical only of the station nearest to the epicenter (Petropavlovsk).

13.2 Microseismic data

The Sumatra earthquake ($M > 9$), which caused a destructive tsunami, is one of the strongest events in the entire history of instrumental seismic observations. In this context, it was of interest to analyze whether this earthquake was preceded by short-term anomalous phenomena in the structure of microseisms similar to those detected before the Kronotskii earthquake. The RAS Geophysical Survey provided data from broadband IRIS stations located around the epicenter of the Sumatra earthquake (Fig. 13.2). The epicenter had the coordinates (3.32° N, 95.85° E), and the coseismic rupture trended mainly NNW for more than 1000 km.

The stations nearest to the epicenter, CHTO in the north and COCO in the south, were located at epicentral distances of 1770 and 1500 km, respectively. The CHTO and KMI stations were closest to the northern end of the rupture (1100 and 1750 km, respectively). Preliminary analysis of records of all stations sampled at a frequency

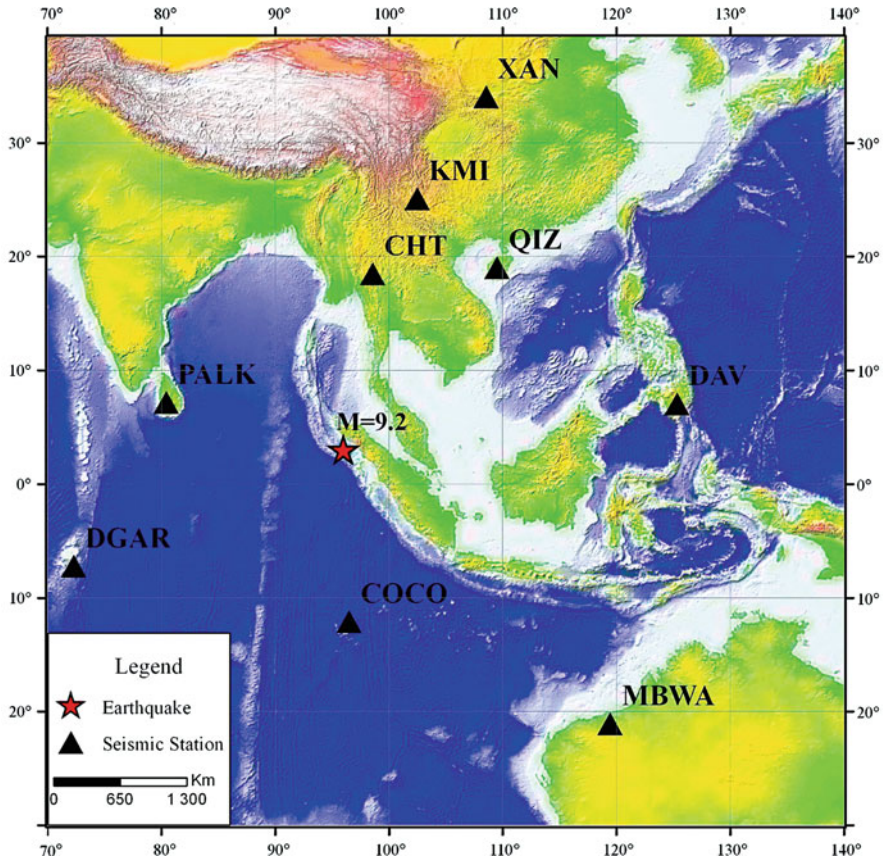

Fig. 13.2 Position of the IRIS stations whose records were analyzed before the Sumatra earthquake. The epicenter of the earthquake is shown by star

of 20 Hz showed that the MBWA station in Australia did not operate during the Sumatra earthquake, the records of the DGAR and PALK stations had defects and gaps, and the DAV and QIZ stations in the Pacific region showed a completely different structure of microseisms as compared with the stations in the Indian Ocean region. Therefore, our analysis was mainly based on data from the CHTO, KMI, XAN, COCO, and (in part) PALK stations. We used records of vertical components with the exception of the COCO station, where this component was not recorded, so that the COCO data on horizontal components were processed. The database used for these stations encompassed the interval of December 16–26, 2004 (the 350th to 360th days from the beginning of the year). Since the Sumatra earthquake occurred at 00:58:54 GMT on December 26, the records of December 26 were processed only up to the first arrival time.

An unusual circumstance was the fact that, 2.5 days prior to the Sumatra earthquake, another strong ($M = 7.9$) earthquake occurred in the southern

hemisphere; its epicenter had the coordinates (49.31° S, 161.35° E) and was located southwest of New Zealand (in the McQuary Ridge area). The vibrations generated by this earthquake were hundreds of times stronger than the microseism level at the aforementioned stations, and surface waves with periods of 300–500 s went around the Earth a few times.

Figure13.3 clearly shows a sequence of such signals, particularly at low noise stations KMI and CHTO. The interval between the successive signals going around

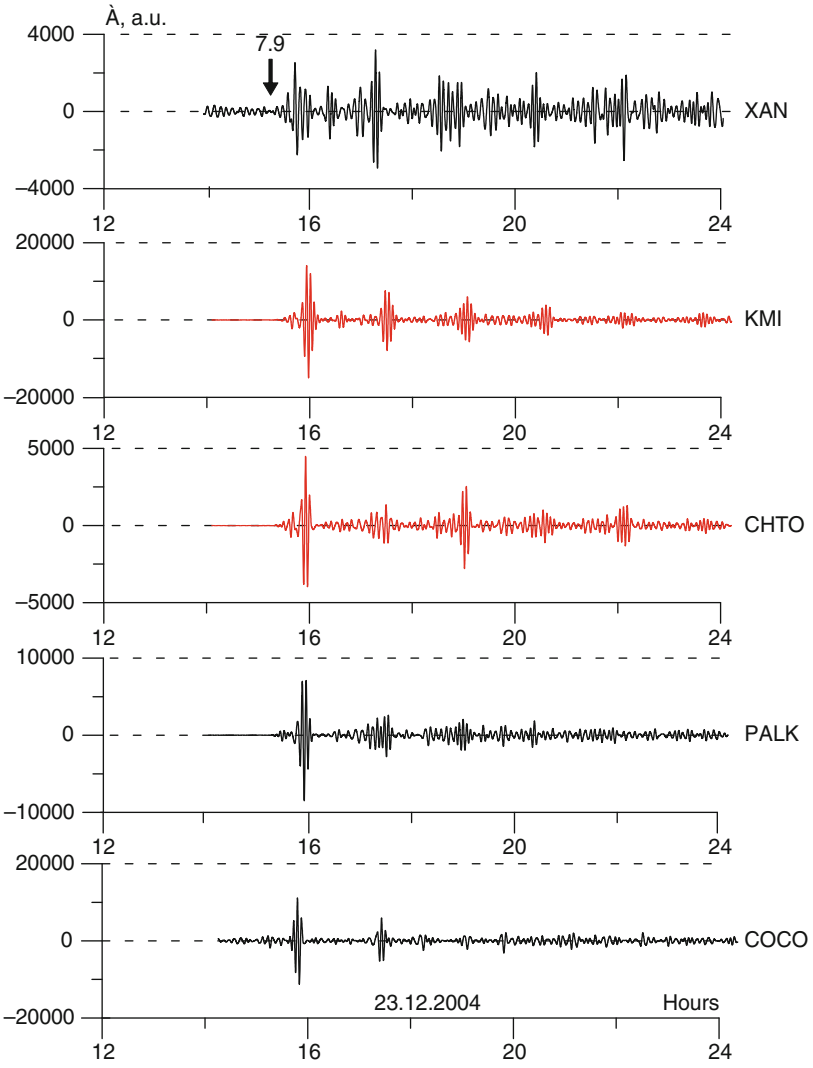

Fig. 13.3 Succession of seismic waves in the range of periods 256–512 min after the McQuary earthquake (marked by an arrow). The station codes are given to the right of the plots, and the station locations are shown in Fig. 13.2

the Earth in both NW and SE directions is 13 h. The records shown in the figure were obtained after aggregation of the signal to a 1-s period, trend removal by smoothing with Gaussian kernels and an averaging radius of 100 samples, and band-pass frequency filtering in the band 256–512 s. The distances from the McQuary earthquake epicenter to the aforementioned stations ranged from 7500 km for the nearest station (COCO) to 10100 km for the farthest station (PALK). Accordingly, the time delay before the arrival of surface waves was about 0.5 h (Fig. 13.3). Vibrations continued actually up to the time of the Sumatra earthquake. Figure 13.4 shows the 10-h record intervals immediately preceding the arrival of waves from this earthquake at the aforementioned stations. The records, from which high frequency components with periods less than 1 min were removed, are dominated by components with periods of 300–500 s but also contain waves with lower and higher frequencies.

13.3 Results

Comparison of wave amplitudes at the same stations shown in Figs. 13.3 and 13.4 reveals the following. Within the time interval of 2.5 days between the McQuary and Sumatra earthquakes, the amplitude of surface waves caused by the first earthquake decreased by a few thousand times at the CHTO, KMI, and PALK stations and only by a few tens of times at the COCO and XAN stations. Possibly, the difference is due to the distinctions in lithosphere quality factors along traces of waves traveling at different azimuths around the Earth. However, one may also assume that the more rapid (by two orders of magnitude) amplitude decrease along the traces of the CHTO, KMI, and PALK stations is caused by anomalously strong absorption of waves in the source area of the future Sumatra earthquake.

Following the aforementioned procedure for identifying hidden periodic oscillations, we checked whether this earthquake was preceded by periodic oscillations in the minute range of microseisms, as was the case before the Kronotskii earthquake. Figures 13.5 and 13.6 present results of the analysis of data from the KMI and CHTO stations. We calculated spectral–temporal plots of $\Delta \ln L(3)$ by processing records of these stations obtained in the period from December 15 to 26 (up to the Sumatra earthquake). The arrows in the figure indicate the times of the Sumatra ($M = 9.2$) and the preceding McQuary ($M = 7.9$) earthquakes. We examined the range of periods from 20 to 60 min with a 180-min window moving at a 60-min step. Prior to the calculations, the low frequency trend was removed by a third-order polynomial. For noise suppression, the calculations were performed only for waves whose amplitude exceeded the median value 1.5. Periodic oscillations arose after the McQuary earthquake and continued for about 24 h. Comparison with Fig. 13.1 reveals a similar effect observed after the foreshock of the Kronotskii earthquake. The records of the XAN, COCO, and PALK stations did not reveal any periodic oscillations. This may be due to a higher noise level, particularly at the XAN and COCO stations, which is evident from comparison of records in Fig. 13.3 with

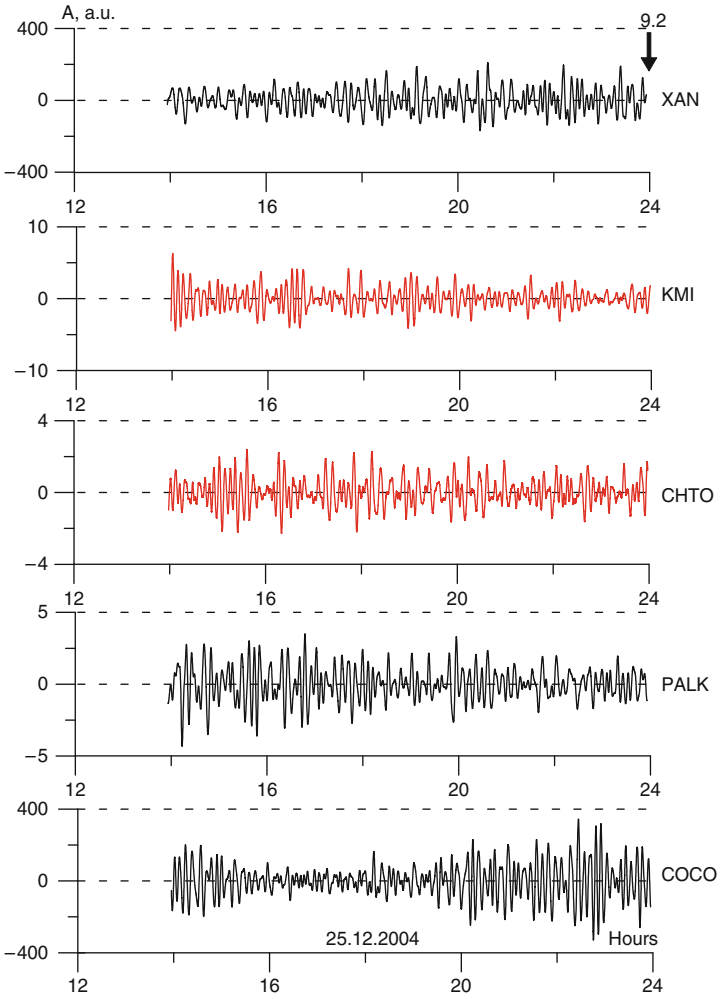

Fig. 13.4 Structure of seismic waves in the range of periods exceeding 1 min recorded 10 h before the Sumatra earthquake. The station codes are given to the right of the plots, and the station locations are shown in Fig. 13.2

amplitudes of surface waves from the McQuary earthquake. In the case of the Sumatra earthquake, we had a few stations located around the source area.

This provided the possibility of testing the hypothesis that the catastrophe was preceded by intensification of collective effects in a nonequilibrium medium, expressed in the synchronization of microseismic vibrations in the region surrounding the earthquake epicenter [Bak et al., 1989; Sornette and Sammis, 1995]. Unfortunately, a recording failure took place at the PALK station in the period between the McQuary and Sumatra earthquakes. Therefore, our analysis used data of only four stations: CHTO, KMI, XAN, and COCO. To analyze the effects of

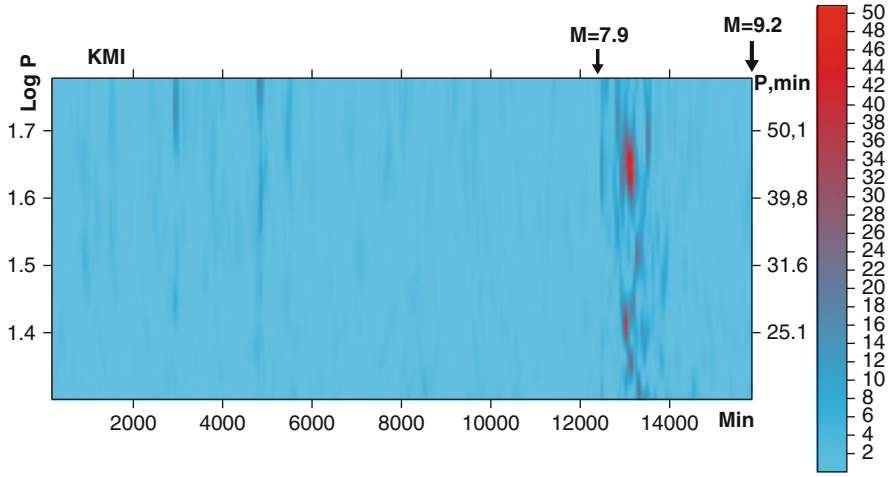

Fig. 13.5 Spectral–temporal diagram of the increment in the logarithmic function of likelihood $\Delta \ln L$ of microseisms recorded at the KMI station before the Sumatra earthquake ($M = 9.2$). The left arrow indicates the time of the McQuary earthquake ($M = 7.9$). The vertical axes show the spectral period (on the right) in minutes and its logarithm (on the left)

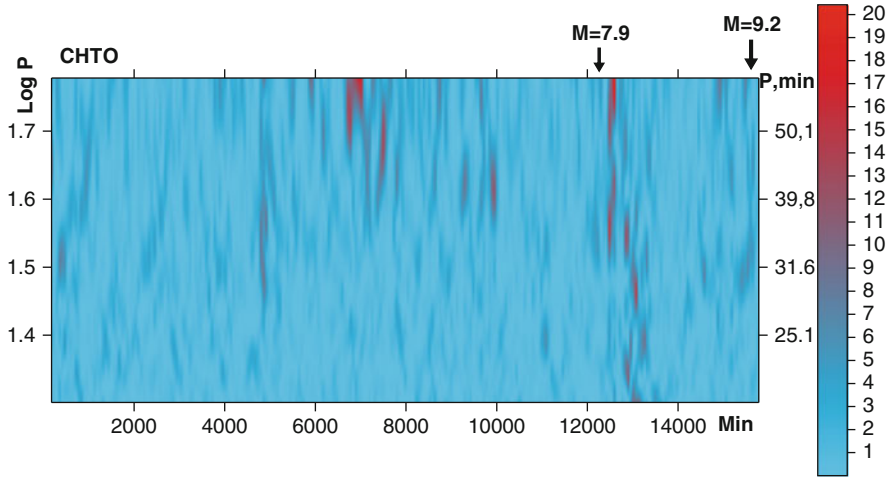

Fig. 13.6 Spectral–temporal diagram of the increment in the logarithmic function of likelihood $\Delta \ln L$ of microseisms recorded at the CHTO station before the Sumatra earthquake ($M = 9.2$). The left arrow indicates the time of the McQuary earthquake ($M = 7.9$). The vertical axes show the spectral period (on the right) in minutes and its logarithm (on the left)

collective behavior in microseismic vibrations at these four stations in the minute range of periods, the initial data sampled at a frequency of 20 Hz were first reduced to a 30-s sampling interval by calculating the averages over successive nonoverlapping intervals 600 samples long. The resulting time series were analyzed by two

approaches based on the calculation of robust wavelet and spectral measures of coherence in the moving time window. The use of different measures aimed to test the stability of the final synchronization effect with respect to different methods of representing the signals: their expansion in strongly nonstationary Haar wavelets and the classic Fourier expansion.

The robust wavelet measure of coherence is a modification of the approach to the analysis of multidimensional time series proposed in [Lyubushin, 2000; Lyubushin and Kopylova, 2004]. The scale-dependent measure of coherent behavior in a moving time window of a given width of N samples is constructed. The analysis is performed independently for each position of the time window (moved to the right by one sample). Before the wavelet decomposition of the analyzed time series fragments present in the current time window, the following sequence of operations is applied to each fragment: (i) the general linear trend within the time window is removed; (ii) a sample estimate of the standard deviation is obtained, and each value is divided by this estimate; (iii) the initial values are converted to the increments between adjacent time values; (iv) the window fragment is complemented with zeros to the full length of $M = \min\{2m : 2m \geq N\}$ samples. Operation (i) removes the strongest low frequency variations in signals, which cannot be statistically representative within the window. The division of each signal within the window by its standard deviation mutually adjusts different time series by reducing the total energy of their variations to the same value. Operation (iii) of the conversion to increments is standard in time series analysis and is intended to enhance the stationarity of sample sets within narrow time windows if low frequencies are predominant. Finally, the last operation (iv) is necessary for the subsequent application of the fast discrete wavelet transform.

Let $q \geq 3$ be the total number of simultaneously analyzed time series, and let τ be the position of the right-hand end of a moving time window N samples wide. We denote as $c_j^{(\beta,\tau)}(k)$ the coefficients of the discrete orthogonal wavelet transform [Mallat, 1998] of the jth time series fragment in the current time window with the position of the right-hand end τ at a detail level of the number β after preliminary operations (i)–(iv). We chose the Haar wavelet from the family of orthogonal wavelets as the most compact and suitable for the analysis of the most abrupt variations in signals. The index k successively enumerates the coefficients belonging to the level $\beta = 1, \ldots, m$. The number m is an exponent of two in the representation $M = 2^m$ such that it is the least number no smaller than the time window width N. At each detail level, the total number of coefficients is equal to $M_\beta = 2^{(m-\beta)}$. Each coefficient $c_j^{(\beta,\tau)}(k)$ reflects the signal behavior in the frequency band $[\Omega_{\min}^{(\beta)}, \Omega_{\max}^{(\beta)}] = [1/(2^{(\beta+1)}\Delta s),\ 1/(2^\beta \Delta s)]$, where Δs is the length of the sampling interval, in the neighborhood of the sample with the number $\tau_k^{(\beta)} = k \cdot 2^\beta$, $k = 1, \ldots, M_\beta$, measured from the position of the left end of the time window. The width of this neighborhood (the temporal "zone of responsibility" of the coefficient) is equal to 2^β. The wavelet transforms yield a set of coefficients $c_j^{(\beta,\tau)}(k)$, $j = 1, \ldots, q$, $\beta = 1, \ldots, m$, $k = 1, \ldots, M_\beta = 2^{(m-\beta)}$. However, some of these coefficients can involve zero values complementing the data set via

preliminary operation (iv). Therefore, the real number of coefficients at the level β reflecting the signal behavior within the window is equal to $L_\beta = 2^{(m-\beta)} \cdot (N/M) = N \cdot 2^{-\beta}$.

Now we address a time series j_0 and construct the measure describing the relationship between this series and all other signals within the current time window. Naturally, this relationship depends on the scale of the variations in question and, therefore, should be sought at various levels of detail between wavelet expansion coefficients. The problem to be solved for this purpose is

$$\sum_{k=1}^{L_\beta} | c_{j_0}^{(\beta,\tau)}(k) - d_{j_0}^{(\beta,\tau)}(k|\gamma)| \rightarrow \min_{\gamma_j}, \quad d_{j_0}^{(\beta,\tau)}(k|\gamma) = \sum_{j=1,\, j\neq j_0}^{q} c_j^{(\beta,\tau)}(k) \cdot \gamma_j \qquad (13.4)$$

We should emphasize that the second sum in (13.4) is a linear combination of expansion coefficients of all time series except the chosen series j_0. Finding the vector γ from the solution of problem (13.4), we obtain certain values of $d_{j_0}^{(\beta,\tau)}(k)$. Now we can find the correlation coefficient between samples of the values of $c_{j_0}^{(\beta,\tau)}(k)$ and $d_{j_0}^{(\beta,\tau)}(k)$ for $k = 1, \ldots, L_\beta$; however, instead of the classic formula for calculating the sample value of the correlation coefficient, we use its robust modification [Huber, 1981], according to which the correlation coefficient between samples $x(k)$ and $y(k)$, $k = 1, \ldots, n$, can be calculated by the formula

$$\rho(x,y) = \frac{S(\breve{Z}^2) - S(\breve{Z}^2)}{S(\breve{Z}^2) + S(\breve{Z}^2)} \qquad (13.5)$$

where $\breve{Z}(k) = a \cdot x(k) + b \cdot y(k)$, $\breve{Z}(k) = a \cdot x(k) - b \cdot y(k)$, $a = 1/S(x)$, $b = 1/S(y)$, $S(x) = med|x - med(x)|$. Here, med(x) is the median of the sample x and, thereby, $S(x)$ is the absolute median deviation of the sample x. Substituting $x(k)$ for $c_{j_0}^{(\beta,\tau)}(k)$, $y(k)$ for $d_{j_0}^{(\beta,\tau)}(k)$, and n for L_β, we obtain the robust value we obtain the robust value $v_{j_0}(\beta,\tau)$ of the correlation coefficient describing the degree of connection of the process $j_0$with all other signals. If we replace in (13.4) the sum of the moduli of deviations by the sum of their squares, the problem can be reduced to the classic Hotelling problem of canonical correlations [Rao, 1965]. Therefore, the quantity $v_{j_0}(\beta,\tau)$ is here referred to as the robust canonical correlation of the time series j_0. The need to replace the classic scheme of the calculation of canonical correlations by its robust variant is dictated by the strong instability of the result of the classic calculations with respect to outliers in wavelet coefficients. The presence of such outliers is due to the well-known fact that the wavelet decomposition is capable of accumulating maximum information about the signal behavior in a relatively small number of wavelet coefficients. We should emphasize that the method is robust in two procedures: the solution of minimization problem (13.4) by the method of least moduli rather than by least squares and the calculation of the correlation coefficient by formula (13.5).

Note that the statistical significance of the estimated robust canonical correlations depends on the number of terms L_β in formula (13.4). Therefore, it is natural to introduce the parameter of statistical significance $L_{\min}$ as the minimum possible value of the number of wavelet coefficients L_β in formulas (13.4) and (13.5) that allows one to calculate correlations at the βth detail level. Thus, it is possible to determine the maximum possible detail level $\beta_{\max}$ defined by the formula $\beta_{\max} = \max\{\beta : L_\beta \geq L_{\min}\}$.

Since, with an increase in the number of the detail level, the number of wavelet coefficients involved in the estimation of $v_k(\beta, \tau)$ exponentially decreases, we reduce statistical fluctuations in estimates by introducing additional averaging over a certain number of coefficients obtained within preceding windows:

$$\bar{v}_k(\tau, \beta) = \sum_{s=1}^{m_\beta} v_k(\tau - s + 1, \beta)/m_\beta, \quad m_\beta = 2^\beta \tag{13.6}$$

The higher the detail level, the deeper the averaging (13.6) over the past time windows; this fact considerably decreases the dependence of the variance of statistical fluctuations in estimation (13.6) on the detail level number and makes this variance nearly the same for different values of β. According to formula (13.6), the effective width of the time window becomes scale-dependent and equal to $N_e^{(\beta)} = N + 2^\beta - 1$.

We define the robust wavelet measure of coherence by the formula

$$\kappa(\tau, \beta) = \prod_{k=1}^{q} |\bar{v}_k(\tau, \beta)| \tag{13.7}$$

The values of measure (7) range from 0 to 1. The larger the value of (13.7), the stronger the overall connection between all analyzed processes on scales corresponding to the number β. We should emphasize that the value of (13.7) is the product of q nonnegative values with moduli less than unity. Therefore, the greater the number q of the series analyzed, the lower the absolute values of $\kappa(\tau, \beta)$. As a consequence, the absolute values of statistic (13.7) can be compared only for the same number of series q. Most interesting are not the absolute values of measure (13.7) but its relative values for different values of τ. Thus, with a fixed Haar wavelet in use, the method has two free parameters: the window width N and the representativeness threshold $L_{\min}$.

The spectral measure of coherence was proposed in [Lyubushin, 1998] (see also [Lyubushin and Sobolev, 2006]) and is based on the use of canonical coherences, which extend the notion of the spectrum of coherence to the situation where, instead of a pair of scalar time series, it is necessary to investigate the relationship between two vector time series at various frequencies: an m-dimensional series $X(t)$ and an n-dimensional series $Y(t)$. The quantity $\mu_1^2(\omega)$, which is called the squared modulus of the first canonical coherence of the series $X(t)$ and $Y(t)$ and is used in this case

instead of the ordinary coherence spectrum, is calculated as the maximum eigenvalue of the matrix [Brillinger, 1975; Hannan, 1970]

$$U(\omega) = S_{xx}^{-1}(\omega) \cdot S_{xy}(\omega) \cdot S_{yy}^{-1}(\omega) \cdot S_{yx}(\omega). \tag{13.8}$$

Here, t is the discrete time enumerating successive samples; ω is the frequency; $S_{xx}(\omega)$ is the spectral $m \times m$ matrix of the time series $X(t)$; and $S_{xy}(\omega)$ is a cross-spectral rectangular $m \times n$, matrix, $S_{yx}(\omega) = S_{xy}^{H}(\omega)$, where the superscript H means Hermitian conjugation.

The component canonical coherences $v_i^2(\omega)$ of the q-dimensional time series $Z(t)$ $(q \geq 3)$are defined as the squared moduli of the first canonical coherence if the series $Y(t)$ in (13.8) is the ith scalar component of the q-dimensional series $Z(t)$ and the series $X(t)$ is the $(q–1)$-dimensional series consisting of the other components. Thus, the quantity $v_i^2(\omega)$ characterizes the correlation at the frequency $\omega \cdot \omega$ of variations in the ith component with variations in all of the other components. We define a frequency-dependent statistic $\lambda(\omega)$ characterizing the correlation at the frequency. ω between variations in all components of the vector series $Z(t)$:

$$\lambda(\omega) = \prod_{i=1}^{q} v_i(\omega) \tag{13.9}$$

Note that, by definition, the values of $\lambda(\omega)$ lie within the interval [0, 1] and the closer the value of $\lambda(\omega)$ to unity, the stronger the correlation between variations in the components of the multidimensional time series $Z(t)$ at the frequency ω. If $q = 2$, measure (13.9) is the ordinary squared modulus of the coherence spectrum. In order to estimate the temporal variability in the measure of interaction between the recorded processes, it is necessary to perform calculations in a moving time window of a given width. Let τ be the time coordinate of a window N samples wide. Calculating the spectral matrices for samples in the time window τ, we obtain the two-parameter function $\lambda(\tau, \omega)$, whose peaks define frequency bands and time intervals of enhanced collective behavior of the jointly analyzed processes.

To implement this algorithm, it is necessary to have in each time window the estimated spectral $q \times q$ matrix $S_{zz}(\tau, \omega)$. Below, we use the model of vector autoregression [Marple, 1987]:

$$Z(t) + \sum_{k=1}^{p} A_k \cdot Z(t-k) = e(t) \tag{13.10}$$

Here, A_k is the $q \times q$ matrix of autoregressive parameters; p is the order of autoregression; and $e(t)$ is the q-dimensional time series of the remainders of identification, which is assumed to be a series of independent Gaussian vectors with a zero mean and an unknown covariance matrix P. Model (13.10) is estimated after the preliminary operations of the elimination of the general linear trend,

transition to increments (in order to increase the stationarity within narrow time windows), and normalization of each scalar component to the unit variance. These operations are performed independently in each time window and for each scalar component of the multidimensional series. The spectral matrix is estimated by the formula

$$S_{zz}(\omega) = F^{-1}(\omega) \cdot P \cdot F^{-H}(\omega), \quad F(\omega) = I + \sum_{k=1}^{p} A_k \cdot \exp(-i\omega k) \qquad (13.11)$$

Estimation (13.11) has a good resolution in frequency for short samples. In the calculations, p was determined by the trial method as a minimum value such that the further increase does not lead to a significant change in the main features of the behavior of the dependence $\lambda(\tau, \omega)$. Everywhere below, we use the value $p = 3$. Thus, we see that the coherence measures $\kappa(\tau, \beta)$ and $\lambda(\tau, \omega)$ are constructed according to the same principle but differ significantly in the signal representation modes. Figures 13.7 and 13.8 plot estimates of these measures in a 12-h-wide moving time window (1440 30-s samples). The wavelet measure $\kappa(\tau, \beta)$ was estimated with the use of the Haar wavelet and the representativeness threshold equal to $L\min = 16$. In estimating the spectral measure $\lambda(\tau, \omega)$, the windows were shifted at a 1-h step (120 samples).

Analysis of the plots in Fig. 13.7 leads to the following conclusions. The wavelet measure of coherence $\kappa(\tau, \beta)$ drops after a seismic event; this is true of both the McQuary event preceding the Sumatra earthquake and the Sumatra earthquake itself. However, beginning from the 12 800-min time mark, the measure of coherence at all levels increases; at the fifth to sixth detail levels, this increase exhibits an obvious positive trend up to the time moment of the shock. At lower detail levels, the measure of coherence reaches peak values approximately 1000–1500 min before the earthquake. Moreover, with increasing detail level number, or "period," the peak of the coherence measure migrates toward the time moment of the shock; i.e., the migration tends to increase the period.

The frequency–time diagram for the spectral measure of coherence $\lambda(\tau, \omega)$ in Fig. 13.8 independently confirms this conclusion; moreover, as the spectral approach makes it possible to trace more smoothly the frequency migration of the coherence measure, Fig. 13.8 even more clearly displays the effect of the migration of the coherence measure from high to low frequencies. However, the approach using wavelet decomposition is more effective for "very low frequencies" (periods longer than 10 min, detail levels 5 and 6 in Fig. 13.7). Thus, the application of both methods of calculating the coherence revealed the scenario of synchronization, which consists in the migration of the fundamental period (or time scale in the wavelet analysis), characterized by maximum collective behavior, from short to long periods.

Further, we attempted to identify asymmetry in the pulsed microseismic oscillations recorded before the Sumatra earthquake at the aforementioned stations. By asymmetry, we mean unequal amplitudes of positive and negative oscillation

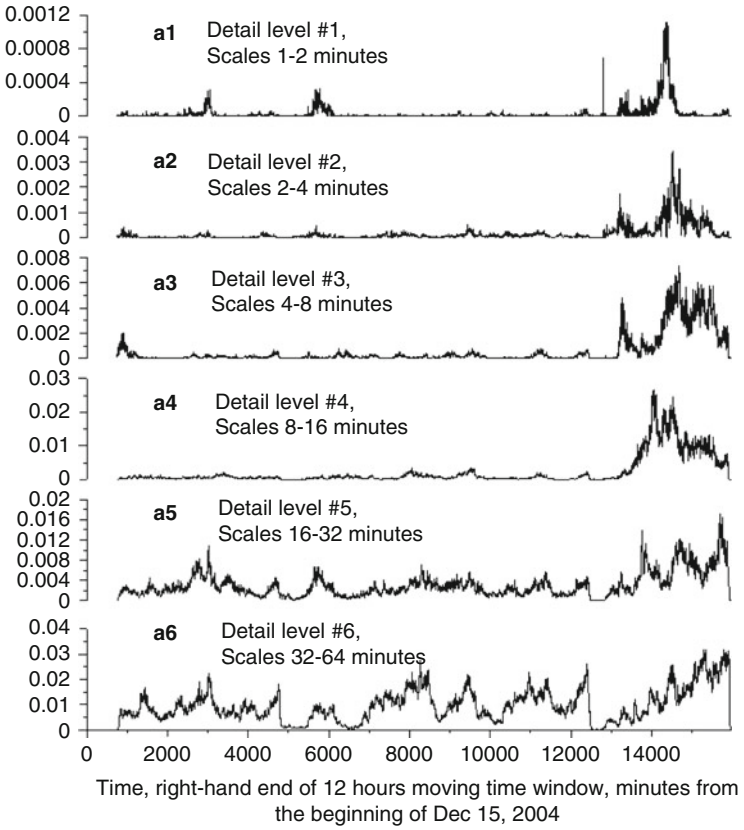

Fig. 13.7 Evolution of the robust wavelet measure of coherence $\kappa(\tau, \beta)$ calculated with a 12-h wide moving time window of 1440 samples from XAN, KMI, CHTO, and COCO records after transition to a 30-s sampling interval. The Haar wavelet was used with a representativeness threshold of $L\min = 16$. The series were preliminarily converted to increments. Plots (a1–a6) relate to detail levels 1–6, which correspond to time scales (periods, the parameter β) of 1–2, 2–4, 4–8, 8–16, 16–32, and 32–64 min. Time measured in minutes from the beginning of December 15, 2004, is plotted on the horizontal axis and corresponds to the right-hand end of the 12-h-wide moving time window τ of 1440 samples; the last time mark is 15975 min, i.e., 02:15 on December 26, 2004

phases, what was clearly expressed in the case of the Kronotskii earthquake [Sobolev et al., 2005]. For this purpose, a program of their automatic identification was developed (it was used in [Sobolev and Lyubushin, 2006]). Since the pulses of interest belong to the middle range of periods, it was necessary first to pass from the initial 0.05-s sampling interval to 1 s and then to eliminate low frequency (including tidal) effects on records and (after the transition to 1-s sampling) high frequency noise. These preliminary operations were effected through averaging and 20-fold downsampling of records, removal of the low frequency Gaussian trend with the scale parameter $H = 1000$ samples (seconds), and subsequent calculation of the

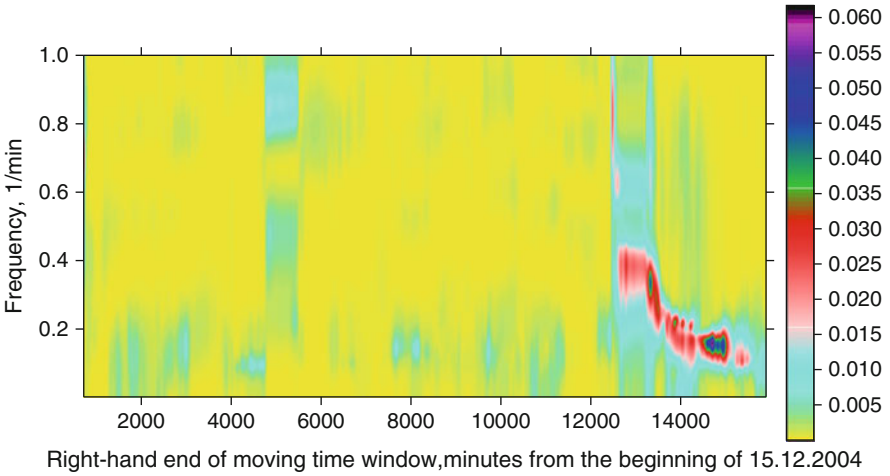

Fig. 13.8 Evolution of the spectral measure of coherent behavior $\lambda(\tau, \omega)$ calculated from XAN, KMI, CHTO, and COCO records after transition to 30-s sampling intervals. The estimation is made in a 12-h-wide moving time window for 1440 samples with a reciprocal shift of 120 samples (1 h) strictly before the arrival from the Sumatra earthquake (AR(3) model and transition to increments). The last time mark is 15900 min, or 01:00 on December 26, 2004

Gaussian trend with a scale parameter of 100 s. We should emphasize that the trend is first removed at $H = 1000$ s, after which deviations from the trend are removed at $H = 100$ s.

These preliminary operations yielded a signal with a sampling interval of 1 s whose power spectrum lay in the range of periods approximately from 200 to 2000 s. It was necessary to automatically identify high amplitude pulses in this signal. For this purpose, after the direct Haar wavelet transform [Mallat, 1998], we left only a small preset part $(1 - \alpha)$ of the wavelet coefficients with maximum moduli (the positive parameter $\alpha < 1$ can be referred to as the compression level), while the remaining coefficients were set to zero. Then, we performed the inverse wavelet transform, yielding a sequence of pulses of sufficiently high amplitudes that are usually separated by intervals of constant values previously filled with noise. This operation is known as denoising in wavelet analysis. The selection of the Haar wavelet for this operation is dictated by the simplicity of the subsequent automatic identification of rectangular pulses. The choice of the compression level determines the number of pulses being identified and the degree of denoising. Note that a signal processed in this way already contains a sufficiently large number of wavelet coefficients that are close or even equal to zero, simply because it was obtained by the preliminary operations of the trend identification and removal. In addition, the compression level obviously depends on the length of the data set because the larger the set, the greater the number of coefficients.

In the time interval from December 15 to 26, we processed 24 h long sampling sets (in all 86400 1-s samples) from all stations. The compression level was 0.9995, yielding about 30 pulses per day. We then calculated the number of pulses of

negative and positive polarities; the two calculation runs included, respectively, all pulses and the most significant pulses with amplitudes exceeding $1m$, where m is the median of their distribution. Since the majority of high amplitude vibrations with periods of 300–500 s were caused by the McQuary earthquake, the analysis was conducted both in the range 200–2000 s and, with the suppression of these waves, in the range 600–2000 s. In both cases and for all stations, we could not detect any significant asymmetry in the shape of the pulses. On the whole, as can be seen from Figs. 13.3 and 13.4, vibrations of positive and negative polarities are symmetric relative to the zero line.

13.4 Discussion

Before the Sumatra earthquake, we did not detect any asymmetry in microseismic amplitudes in the minute range of periods, as was observed before the Kronotskii and Neftegorsk events [Sobolev et al., 2005; Sobolev and Lyubushin, 2006]. We relate the asymmetry, expressed as the difference between amplitudes of positive and negative polarities, to the imperfect elasticity of rocks containing fractures. This is confirmed by laboratory experiments in which a sinusoidal signal is distorted during its propagation through a sample subjected to deformation [Sobolev and Ponomarev, 1997]. Phases of compressive and tensile stresses under these conditions cause different deformations due to the difference in the strain moduli under compression and extension. One should assume that either the lithospheric region near the stations surrounding the source of the Sumatra earthquake did not possess imperfect elasticity of this type or the epicentral distances (more than 1000 km) were too great for this effect to be reflected in records of the stations. However, as noted above, the attenuation of the surface waves produced by the McQuary earthquake increased during their repeated propagation near the CHTO, KMI, and COCO stations. A possible interpretation of the absence of wave asymmetry notwithstanding significant wave attenuation is that the latter is caused by an increase in the damping decrement due to an increase in the plasticity or water saturation in the source area of the forthcoming Sumatra earthquake. The difference between moduli under compression and extension conditions in plastic media is known to decrease with increasing plasticity of the consolidated medium subjected to deformation [Malinin, 1968].

As was noted in [Sobolev, 2004; Sobolev et al., 2005], foreshocks can provoke periodic oscillations near the epicentral area of a future strong earthquake. This phenomenon is a feature indicating an unstable state of the lithosphere. The analysis of the Sumatra earthquake confirmed, to an extent, this hypothesis, with the McQuary earthquake acting as a foreshock (Figs. 13.5, 13.6). This effect was also observed before the Kronotskii earthquake, which occurred 27 days after an earthquake in Tibet with $M = 7.7$. During 3.5 h after the latter, the Petropavlovsk station on Kamchatka recorded waves with periods of a few tens of minutes [Sobolev, 2004].

The second effect that was clearly observed before the Sumatra earthquake was a gradual decrease in the predominant periods of premonitory vibrations in the range from a few minutes to tens of minutes (Figs. 13.7, 13.8). Under the assumption of an intraterrestrial mechanism of these vibrations, they can be related to resonance effects in lithospheric blocks of increasingly larger scales and/or in lithospheric and deeper layers of the Earth. The analysis of microseismic amplitudes in the second range of periods showed that, at all of the aforementioned stations in the time interval from December 15 to 26, the microseismic level was virtually stationary, thereby ruling out the influence of atmospheric effects. This phenomenon was previously noted in the range of very long periods (of the order of one year) in the analysis of a seismic catalog and in a laboratory experiment involving deformation and failure of a sample [Sobolev, 2003]; apparently, this is a fundamental property of a nonequilibrium system approaching instability. In the case of the Sumatra earthquake, the instability could have been triggered by the McQuary earthquake, which caused propagation of deformation waves along the future Sumatra rupture [Nikolaevskii, 1996]. A theoretical substantiation of the decrease in the period of oscillatory processes in the same place of the lithosphere was proposed by Dubrovskii [1988], who proved the following theorem. If a system with a set of characteristic critical parameters is in an unstable equilibrium separating the steady- and unsteady-state ranges of parameters, then the steady-state system will produce waves whose frequency tends to zero if the system approaches the critical state of unstable equilibrium and the dimensions of wave disturbances are finite. Dubrovsky and Dieterich [1990] extended this approach to the case of deformation waves propagating along a fault (trapped waves), giving rise to instable slip of fault walls relative to each other. The development of this instability (an earthquake or creep) is preceded by a decrease in the frequency of these waves.

One cannot exclude the mechanism by which the waves under discussion originate as a result of selforganization of the source area. The appearance of rhythms is a common phenomenon in the evolution of nonequilibrium systems [Nicolis and Prigogine, 1977]. If waves in blocks of different sizes are described by nonlinear equations of the type (13.12) containing chaotic and periodic components, and K is the coupling coefficient (e.g., between stresses in the blocks), such systems will show the effects of phase synchronization and the frequency ω range of synchronization widens with an increase in K [Ott, 2002].

$$dx/dt = F(x) + K^{*}P(\omega t) \tag{13.12}$$

One may suppose that the degree of the mutual influence of blocks (or seismically active faults) increases as macroscopic instability (an earthquake) is approached. This is accompanied by enlargement of the geometric region of collective behavior, in agreement with the concept of self-organized seismic criticality [Bak et al., 1989; Sornette and Sammis, 1995]. In this case, the spectrum of vibrations can evolve into the lower frequency range. We realize that, to gain more substantiated ideas of the physical mechanisms responsible for the phenomena

discussed in this paper, additional (and not only seismological) investigations are required.

13.5 Conclusion

The analysis of records obtained at a few stations 60 h before the Sumatra earthquake revealed periodic vibrations in the range of periods from 20 to 60 min that arose after the McQuary earthquake and continued for about 24 hours. This phenomenon was previously observed after the foreshocks preceding the Kronotskii earthquake.

Synchronization of vibrations recorded at the stations began 53 h before the Sumatra earthquake and continued up to its onset time, with the predominantperiod gradually increasing from a few minutes to tens of minutes.

These phenomena are consistent with the hypothesis according to which the radius of correlation and collective effects in the microseismic field increases prior to an earthquake within the framework of the concepts of self-organized seismic criticality.

References

Bak P., S. Tang, and K. Winsenfeld, "Earthquakes As Self-Organized Critical Phenomenon," J. Geophys. Res. **94**, 15 635–15 637 (1989).

Brillinger D. R., Time Series. Data Analysis and Theory (Holt, Rinehart and Winston, New York, 1975).

Dubrovskii V.A., "Tectonic Waves and Contemporary Movements," in Lithosphere of Central and Eastern Europe: Geodynamics (Naukova Dumka, Kiev, 1988) [in Russian].

Dubrovskiy V.A. and J. Dieterich, "Wave Propagation along Faults and the Onset of Slip Instability," EOS **71**(17), 635–636 (1990).

Hannan E.J., Multiple Time Series (Wiley, New York, 1970).

Huber R.J., Robust Statistics (Wiley, New York, 1981).

Lyubushin A.A., "Analysis of Canonical Coherences in the Problems of Geophysical Monitoring," Fiz. Zemli, No. 1, 59–66 (1998) [Izvestiya, Phys. Solid Earth **34**, 52–58 (1998)].

Lyubushin A.A., "Wavelet-Aggregated Signal and Synchronous Peaked Fluctuations in Problems of Geophysical Monitoring and Earthquake Prediction," Fiz. Zemli, No. 3, 20–30 (2000) [Izvestiya, Phys. Solid Earth **36**, 204–213 (2000)].

Lyubushin A.A., "Periodicities and Rhythms of Global Seismicity in the 20th Century," in Joint Session"Rhythmicity and Cyclicity in Geology As Evidence for General Laws of Development" of the OGGGGN RAN Scientific Workshop "Theoretical Problems of Geology" and the X Workshop "System of the Planet Earth," February 7 and 8, 2002, Abstracts (OGGGGN RAN, Moscow, 2002), pp. 66–67 [in Russian].

Lyubushin A.A., V.F. Pisarenko, V.V. Ruzhich, and V. Yu. Buddo, "Extraction of Periodicities in the Seismic Regime," Vulkanol. Seismol., No. 1, 62–76 (1998).

Lyubushin A.A. and G.N. Kopylova, "Multidimensional Wavelet Analysis of Time Series of Electrotelluric Observations in Kamchatka," Fiz. Zemli, No. 2, 82–96 (2004) [Izvestiya, Phys. Solid Earth **40**, 163–176 (2004)].

Lyubushin A.A. and G.A. Sobolev, "Multifractal Measures of Synchronization of Microseismic Oscillations in aminute Range of Periods," Fiz. Zemli, No. 9 (2006) [Izvestiya, Phys. Solid Earth **42**, 734–744 (2006)].

Malinin N.N., Applied Theory of Plasticity and Creep (Mashinostroenie, 1968) [in Russian].

Mallat S., A Wavelet Tour of Signal Processing (Academic, San Diego, 1998).

Marple, Jr. S.L., Digital Spectral Analysis with Applications (Prentice-Hall, Englewood Cliffs, 1987).

Nicolis G. and I. Prigogine, Self-Organization in Non-Equilibrium Systems (Wiley, New York, 1977; Moscow, Mir, 1979) [in Russian].

Nikolaevskii V.N., Geomechanics and Fluid Dynamics (Nedra, Moscow, 1996) [in Russian].

Ott E., Chaos in Dynamic Systems (University Press, Cambridge, 2000).

Rao S.R., Linear Statistical Inference and Its Applications (Wiley, New York, 1965).

Sobolev G.A., "Microseismic Variations Prior to a Strong Earthquake," Fiz. Zemli, No. 6, 3–13 (2004) [Izvestiya, Phys. Solid Earth **40**, 455–464 (2004)].

Sobolev G.A. and A.V. Ponomarev, "The Vibratory Effect on the Fracture Process and Acoustic Regime in a Fault Zone Model," Vulkanol. Seismol., No. 6, 51–57 (1997).

Sobolev G.A., A.A. Lyubushin, and N.A. Zakrzhevskaya, "Synchronization of Microseismic Variations within a Minute Range of Periods," Fiz. Zemli, No. 8, 3–27 (2005) [Izvestiya, Phys. Solid Earth **41**, 599–621 (2005)].

Sobolev G.A. and A.A. Lyubushin, "Microseismic Impulses As Earthquake Precursors," Fiz. Zemli, No. 9 (2006)Izvestiya, Phys. Solid Earth **42**, 721–733 (2006)].

Sobolev G.A. and A.A. Lyubushin, "Microseismic Anomalies before the Sumatra Earthquake of December 26, 2004," Fiz. Zemli, No. 5, 3–16 (2007) [Izvestiya, Phys. Solid Earth 43, 341–353 (2007)].

Sornette D. and C.G. Sammis, "Complex Critical Exponents from Renormalization Group Theory of Earthquakes: Implications for Earthquake Predictions," J. Phys. I. France **5**, 607–619 (1995).